Quantum fluctuations and the magnetic ground state of $Ce_3Pd_{20}Si_6$

P. P. Deen,[1] A. M. Strydom,[2] S. Paschen,[3] D. T. Adroja,[4] W. Kockelmann,[4] and S. Rols[1]
[1]*Institut Laue-Langevin, 6 rue Jules Horowitz, 38042 Grenoble, France*
[2]*Physics Department APK, University of Johannesburg, P.O. Box 524, Aukland Park 2006, South Africa*
[3]*Institut für Festkörperphysik, TU Wien, Wiedner Hauptstr. 8-10/138, A-1040 Wien, Austria*
[4]*ISIS Facility, Rutherford Appleton Laboratory, Chilton, Didcot, Oxon OX11 0QX, United Kingdom*
(Received 27 October 2009; revised manuscript received 5 January 2010; published 24 February 2010)

The temperature and magnetic field dependence of neutron-scattering studies on the heavy fermion compound $Ce_3Pd_{20}Si_6$ are reported. Inelastic neutron scattering reveals two crystal-field excitations corresponding to the environments of the two distinct rare-earth locations within this cubic compound. Surprisingly, the ground states of the two individual Ce sites are inequivalent with the 4*a* site having a Γ_7 ground state, while the 8*c* site reveals a Γ_8 ground state. This is in contrast to the situation found in the analogous compound $Ce_3Pd_{20}Ge_6$, where the Γ_8 ground state is realized for both Ce sites. In addition, these results reveal an interaction between the 8*c* and 4*a* sites previously believed to be absent. The ground state was probed with uniaxial polarization analysis across the region in which field-induced quantum criticality has previously been determined. In zero applied magnetic field no long-range magnetic order could be determined. However, further evidence of field-induced quantum criticality is presented with the observation of diffuse scattering consistent with quantum fluctuations due to nearest-neighbor spin correlations between the two Ce sites.

DOI: 10.1103/PhysRevB.81.064427 PACS number(s): 75.20.Hr, 71.27.+a, 71.70.Ch, 78.70.Nx

I. INTRODUCTION

Interest in phase space close to a quantum critical point (QCP) stems from the belief that novel phases may be uncovered via zero-point quantum fluctuations inherent at a QCP.[1,2] It is therefore of great importance to understand the static and dynamic spin order in compounds exhibiting quantum critical phenomena. Quantum fluctuations that occur at a QCP can induce substantial variations in the strongly correlated electronic order of the compounds. As such it is not surprising that QCPs are often associated with heavy fermion behavior exhibiting non-Fermi-liquidlike properties. The caged compound $Ce_3Pd_{20}Si_6$ (CPS) is regarded as one of the heaviest electron Kondo systems,[3] with the low-temperature specific heat reaching $C_P/T=8$ J/(mol Ce K^2) in comparison to the prototype Kondo compound $CeCu_6$ in which $C_P/T=1.6$ J/(mole Ce K^2).[4] Such high specific-heat values are often interpreted as arising from strong electronic correlations. Indeed a recent study on CPS uncovered a field-induced QCP[5] indicating a most unusual ground state that originates from conduction electrons acquiring huge effective masses or, in the Kondo picture, from a very large and sharp electronic density of states at the Fermi energy through the Kondo resonance.

CPS is a member of the clathrate ternary intermetallic series $REPd_{20}Ge_6$ and $REPd_{20}Si_6$, (*RE*=rare earth), a fascinating class of materials with potential for low-temperature thermoelectric applications[6] due to reduced thermal conductivity via rattling of the rare-earth atoms while maintaining the electrical conductivity. Structurally the magnetic *RE* atoms are positioned at two cubic sites, Wyckoff 4*a* (face centered cubic) and 8*c* (simple cubic) of the structure $Fm\bar{3}m$,[7] see Fig. 1. The phase diagrams of the Ge-based compounds show common features, with two antiferromagnetic transitions observed at T_L and T_U, $T_L<T_U$ in the Nd-, Sm-, Gd-, Tb-, Dy-, and Ho-based compounds.[8] These transitions accompany the ordering of the two rare-earth sites with 8*c* ordering at T_U into a $\mathbf{k}_2=[1\ 1\ 1]$ structure and 4*a* ordering at the lower temperature T_L into a $\mathbf{k}_1=[0\ 0\ 1]$ structure.[9–12]

The interatomic separation of the 8*c* and 4*a* sites are approximately 6.1 and 8.6 Å, respectively. It can therefore be argued that the interatomic separation is responsible for the temperature at which the order occurs, T_L for the ordering of the 8*c* atoms with 6.1 Å interatomic distance and the higher temperature transition T_U is due the ordering of the 4*a* sites with interatomic distance of 8.6 Å. However it is unusual that there is no intersite, 4*a*-8*c*, magnetic correlations since the different sites are only separated by 5.4 Å and yet do not couple magnetically in any of the above-mentioned compounds.[9–12]

Replacing the heavier rare earths with Ce drastically alters the behavior of these phase transitions. $Ce_3Pd_{20}Ge_6$, the isoelectronic compound to CPS, reveals a pair of magnetic phase transitions by specific-heat measurements at $T_L=0.7$ and $T_U=1.2$ K.[13] Only the lower transition, T_L, presented an anomaly in the ac-susceptibility data. Neutron diffraction verified the antiferromagnetic ground state below T_L correlating the Ce 4*a* moments with wave-vector transfer $\mathbf{k}_1=[0\ 0\ 1]$.[14] However, the transition at T_U was ascribed to a quadrupolar transition due to the high value of the mag-

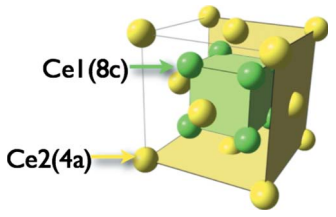

FIG. 1. (Color online) Crystal structure of $Ce_3Pd_{20}Si_6$. For clarity only the Ce atoms are shown. Green atoms show the Ce 8*c* sites and yellow atoms show the Ce 4*a* sites.

netic entropy.[13] Ultrasonic and dilatometric methods determined T_U to be the onset of ferroquadrupolar order accompanied by a tetragonal or orthorhombic distortion[15] involving a Γ_8 ground state on both crystallographic sites.

The first indication of magnetic ordering in CPS was based on the sharp cusp at T_U=0.15 K from ac susceptibility[3] in a small applied field. At the same time, the low-temperature phase transition was tentatively assigned to spin-glass ordering due to the existence of a remnant magnetic moment.[3] Initial exploratory studies of muon-spin resonance (μSR) at intermediate temperatures[16] sought to describe the magnetic behavior of CPS in terms of molecular magnetism on account of the two interleaved Ce sublattices in this compound. Strydom *et al.*[5] clearly demonstrated two distinct phase transitions in CPS at 0.31 and 0.5 K via specific-heat measurements in zero field. The determined high-temperature effective magnetic moment $\mu_{eff}=2.6\mu_B$ was slightly greater than the free-ion moment of Ce^{3+}, $\mu_{free}=2.54\mu_B$, with a Weiss temperature of −21 K that indicates antiferromagnetic correlations. The two transitions show opposite behavior in applied fields. The transition at T_U shifts upward in temperature and becomes indeterminate for fields above 8 T.[5] T_L, on the other hand, shifts downwards in temperature and disappears in fields above 1 T. Around the critical field of 1 T the electrical resistivity changes from Fermi-liquid $[\rho(T)\sim AT^2]$ to non-Fermi-liquidlike $[\rho(T)\sim T]$ which, together with the observed growth in the A coefficient near the critical field, signals the onset of a field-induced QCP.[17]

To date the spin-correlated behavior found in CPS has been investigated by resistivity, specific-heat and ultrasonic measurements. We have performed neutron inelastic scattering and polarized neutron-diffraction experiments to characterize the ground state of CPS and to obtain spatial information on the magnetic field dependence of the low-temperature phases. Our results have a broader relevance to the various open questions and fundamental issues of the physics of quantum criticality that are presently receiving wide-spread attention in the literature.

II. RESULTS AND DISCUSSION: INELASTIC AND ELASTIC NEUTRON SCATTERING

The electrostatic potential arising from the electric-charge distribution surrounding a rare-earth ion, the crystalline electric field (CEF), splits the ground state and excited multiplets. In rare-earth systems, with the notable exception of Eu^{3+} and Sm^{3+}, the CEF splitting between the ground state into the excited multiplets compared with the intermultiplet energy separation is much larger. The CEF can therefore be described by a perturbation on the $(2J+1)$ degenerate eigenstate of the ground-state multiplet which, in the case of a Ce^{3+} atom sitting in cubic point symmetry, can written as

$$V_{\mathrm{CEF}} = B_4 O_4^0 + 5B_4 O_4^4, \tag{1}$$

where O_4 is the appropriate Stevens operator, given explicitly in,[18–20] and B_4 is the CEF strength surrounding the Ce atom that can be estimated from the analysis of the inelastic neutron-scattering data. Diagonalizing Eq. (1), using the Stevens operators for the Ce^{3+} atom, $J=5/2$, gives a degenerate solution for $\lambda=120B_4$ and a second solution for $\lambda=240B_4$ and thus $\Delta_{\mathrm{CEF}}=\pm 360B_4$.

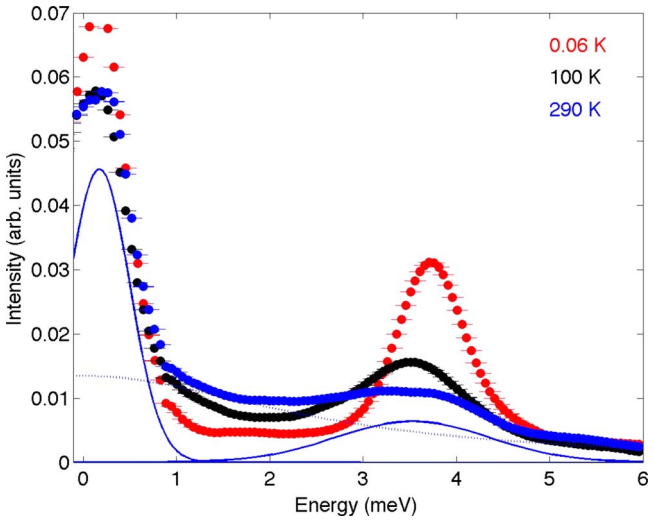

FIG. 2. (Color online) Inelastic neutron-scattering data at 0.06, 100, and 290 K. The full line shows the crystal-field contributions. The dashed line represents the Lorentzian quasielastic line contribution centered at 0 meV.

Inelastic neutron scattering (INS) is an experimental tool that is uniquely disposed toward probing the CEF surrounding a magnetic atom.[21] INS measurements have been performed at the Institut Laue-Langevin, Grenoble, using the thermal time-of-flight spectrometer, IN4 with an incident wavelength of 2.6 Å providing an elastic peak with a full width at half maximum (FWHM) of 0.60(1) meV and covering an energy range $-20<E<10$ meV. Data were collected over a temperature range 60 mK$<T<$290 K. The data were corrected for background and phonon contributions via the subtraction of the scattering from the nonmagnetic isostructural compound $La_3Pd_{20}Si_6$ scaled via the spin incoherent scattering. The detector efficiency was calibrated with a vanadium reference. The energy dependence of the scattering cross-section was obtained by integrating the total scattering cross-section, $S(Q,\omega)$, across the detector angles ensuring that elastic Bragg scattering was excluded.

Two CEF excitations, at 0.31(2) and 3.91(1) meV were uncovered at 60 mK, see Fig. 2. The dependence of the wave-vector transfer of this scattering, with data integrated over energy, follows the Ce^{3+} magnetic form factor within the dipole approximation[22] as expected for CEF excitations. No variation from the dipole approximation due to the onset of the quadrupolar order, expected below 0.5 K, could be detected. The inset of Fig. 3(a) shows the CEF excitation at 0.31(2) meV at 60 mK. The data have been corrected for detailed balance. The dashed line in Fig. 3(a) is a fit to the data with two Lorentzian curves. The existence of the low-energy excitation was initially not clear since it sits very close to the elastic line.[23] Careful subtraction of the background contributions, including components of Bragg scattering, was necessary to reveal the slight broadening of the elastic line due to the CEF excitation at 0.31 meV. The inset of Fig. 3(b) shows the higher energy excitation at 3.91(1)

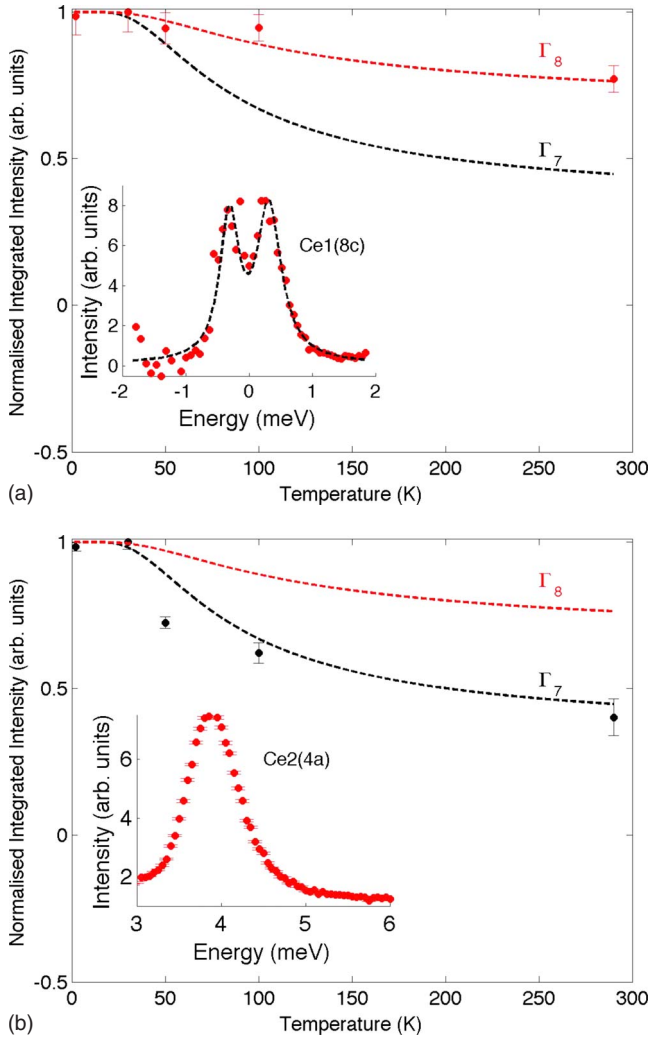

FIG. 3. (Color online) (a) Temperature dependence of the integrated intensity of the low-energy [0.31(2) meV] excitation. Inset: energy dependence of 0.31(2) meV excitation at 60 mK with data corrected for detailed balance. (b) Temperature dependence of the higher energy [3.91(1) meV] CEF transition. Inset shows the energy dependence at 60 mK.

meV. The crystal-field strengths calculated from the observed CEF transitions are therefore B_4=0.00086(6) and 0.106(1) meV for the two Ce sites.

The interaction of an impurity spin with the conduction electrons gives rise to the unusual features of the Kondo or heavy fermion compounds. The relaxation of the impurity magnetic ion results in broad quasielastic scattering with FWHM comparable to the Kondo temperature $\Gamma \sim T_K$[24] for $T \to 0$, an observation that is well documented.[25–27] Resistivity measurements on CPS revealed the importance of the incoherent Kondo effect through the $\rho(T) \propto -\ln(T)$ dependence above 30 K.[3,5] Accordingly the Kondo regime should give rise to quasielastic scattering with Γ_0=30 K =2.59 meV. Figure 2 shows the variation in inelastic scattering between 60 mK and 290 K. At 60 mK the quasielastic contribution is small while at 290 K it is more obvious. The full lines in Fig. 2 represent the scattering from the two CEF excitations at 290 K while the dashed line represents the quasielastic scattering at 290 K centered at 0 meV with a FWHM of 5.23(1) meV. The contributions from the two CEF peaks makes it difficult to determine the temperature dependence of the quasielastic contribution with certainty. Higher resolution data will be required to indicate whether the $\Gamma_0 \sim 30$ K expectation from electrical resistivity measurements is indeed upheld in the quasielastic neutron scattering of CPS.

The scattering cross-section of two excitations should give an approximate 2:1 ratio corresponding to the number of atoms on the Ce1 (8*c*) and Ce2 (4*a*) sites, respectively. The ratio of intensities obtained from the data is approximately 3:1 possibly due to the strong feed through of the elastic line shape to the low-energy peak. The order of magnitude difference is, nevertheless, sufficiently resolved to indicate that the low-energy peak corresponds to the 8*c* sites and thus the high-energy peak is assigned to the 4*a* sites. This is in accordance with results for $Ce_3Pd_{20}Ge_6$ ascribing the higher energy CEF transition to the 4*a* Ce sites.[28]

The temperature dependence of the integrated intensity of the CEF peaks are shown in the main panels of Fig. 3 and can be understood in terms of the ground-state and first-excited-state population factors. The probability that an excited state, **k**, is occupied is given via the grand canonical partition function for a system composed of fermions with 0 or 1 particles in a given state

$$f(E_k) = \frac{1}{1 + \exp(\Delta E)/k_B T}, \tag{2}$$

where ΔE is the excitation energy, k_B is the Boltzmann constant, and T is the temperature. The ground state of a Ce^{3+} ion is split by the spin-orbit coupling to a $^2F_{5/2}$ ground state and, in the case of a cubic point symmetry, this is further split into a quartet Γ_8 or into a doublet Γ_7 ground state by the CEF surrounding the ion. The temperature dependence of the CEF peaks will therefore correspond to either a $\Gamma_8 \to \Gamma_7$ or a $\Gamma_7 \to \Gamma_8$ excitation and their corresponding probabilities are thus given by

$$f(E_k) = [2 + 4\ \exp(\Delta E/k_B T)]^{-1}, \quad \Gamma_7 \to \Gamma_8, \tag{3}$$

$$f(E_k) = [4 + 2\ \exp(\Delta E/k_B T)]^{-1}, \quad \Gamma_8 \to \Gamma_7. \tag{4}$$

The dashed lines in Fig. 3 show the calculated probabilities for both the Γ_7 and Γ_8 ground state with the integrated intensities for the low-energy CEF peak at 0.31 meV in (a) and the higher energy CEF peak at 3.91(1) meV in (b). The ground state of the Ce atoms sitting on the 4*a* and 8*c* sites are therefore Γ_7 and Γ_8, respectively. This has profound implications for the magnetic and multipolar order expected in $Ce_3Pd_{20}Si_6$ with a Γ_7 doublet enabling dipole order only and a Γ_8 quartet enabling dipolar, quadrupolar, and octupolar order. The onset of quadrupolar order is expected to produce a splitting of the Γ_8 CEF excitation. No such splitting was observed, however, it is possible to estimate the upper limit of the splitting in energy. Within statistical error a splitting of approximately 0.24(3) meV or less would not be observed in data. Further higher resolution neutron-scattering studies are

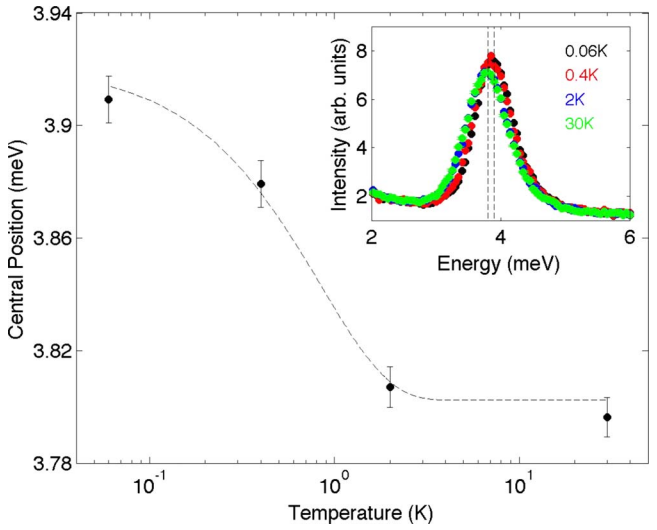

FIG. 4. (Color online) Temperature dependence of the central energy position of the high-energy excitation at 3.91(1) meV. The dashed line is a guide to the eyes. Inset: energy dependence of the scattering at temperatures 0.06, 0.4, 2, and 30 K.

called for to validate such a small-energy splitting at the onset of quadrupolar order in CPS.

The temperature dependence of the energy at maximum intensity of the higher energy CEF peak, with the Γ_7 ground state, is shown in Fig. 4. The position shifts by 0.1 meV between 0.4 and 2 K and thus appears to be linked to the higher temperature transition at T_U=0.5 K. This peak has been assigned to the 4*a* site with a Γ_7 ground state which can only order with dipolar symmetry. However, in comparison with $Ce_3Pd_{20}Ge_6$ this transition, T_U, is due to the ordering of the 8*c* sites and thus the onset of quadrupolar order. These results therefore indicate a first signature of an interaction between Ce atoms occupying the 4*a* and 8*c* sites in these ternary intermetallic compounds.

The results of neutron-diffraction measurements, designed to investigate coherent magnetic order-derived scattering as well as a putative crystal-structure distortion at a possible quadrupolar order in CPS, are shown in Figs. 5(a)–5(c). The experiments were performed at the ISIS Facility of the Rutherford Appleton Laboratories of the UK Science and Technology Facilities Council on the General Materials Diffractometer (GEM), a high-resolution, high-intensity powder diffractometer capable of resolving interplanar spacings of $\Delta d/d \simeq 0.0025$, and on ROTAX, a time-of-flight diffractometer of effective *d*-spacing resolution $\Delta d/d$=0.0035. The three panels represent data collected over the temperature range (a) from 300 K, (b) through 5.5 K, and (c) down to 0.04 K. The solid lines represent full-profile Rietveld refinements of the data to the face-centered cubic space group $Fm\bar{3}m$ (nr 225). It is noted that the initial work of Gribanov *et al.*[7] gave $Fm3m$ as the space group. The change in notation involves a shift in the unit-cell coordinate from x(=0.11) to $\frac{1}{2}-x$ for the 32*f* Wyckoff site in CPS so that the atomic sites can be described using the values of Table I. This is a permissible symmetry operation of this space group[29] which, in this particular case, turns out to be non-

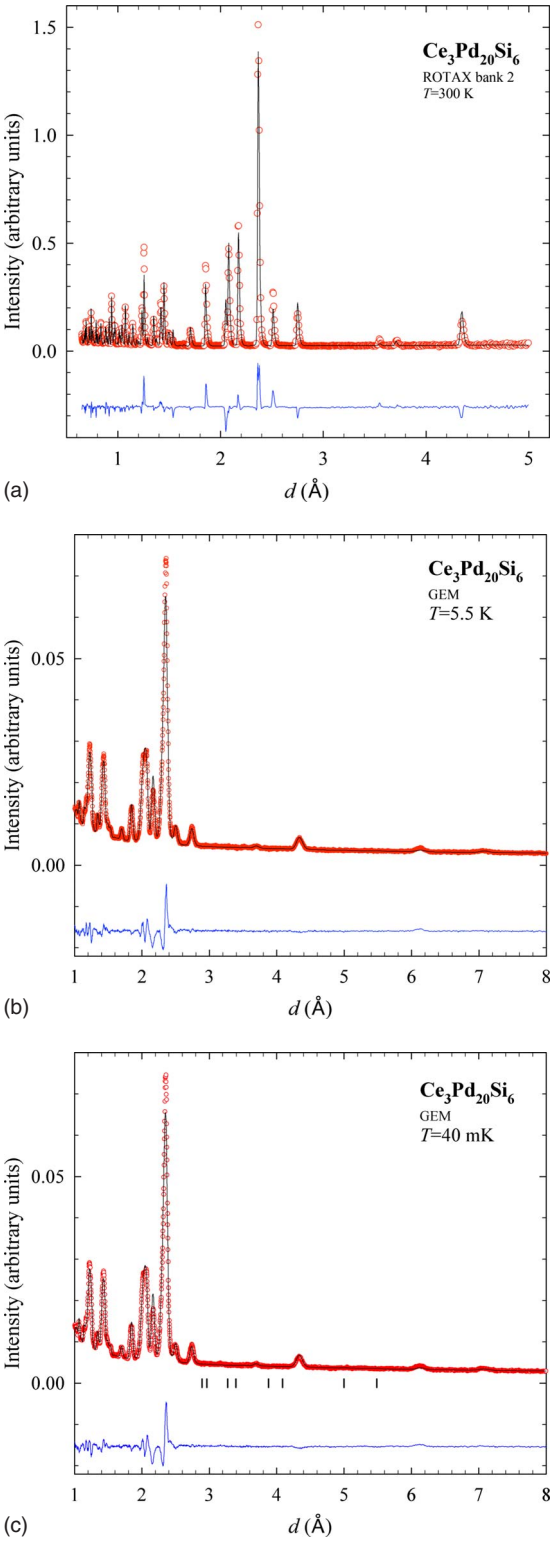

FIG. 5. (Color online) Powder diffraction data with the full-profile Rietveld refinement (full line) of CPS at (a) 300 K, (b) 5.5 K, and (c) 0.04 K. The vertical markers in the low-temperature plot (c) indicate the expected positions of magnetic Bragg diffraction, as discussed in the text.

trivial for predicting the powder diffraction spectrum of $REPd_{20}X_6$-type compounds. The data in Fig. 5 reveal a contraction in the cubic lattice parameter from

TABLE I. Structural parameters for $Ce_3Pd_{20}Si_6$ as discussed in text.

Atom	Site	(x, y, z)	Occupancy
Ce1	4*a*	(0, 0, 0)	1
Ce2	8*c*	$(\frac{1}{4}, \frac{1}{4}, \frac{1}{4})$	1
Pd1	32*f*	(0.38370, *x*, *x*)	1
Pd2	48*h*	(0, 0.176, *y*)	1
Si	24*e*	(0.263, 0, 0)	1

a_0=12.2780(1) Å at 300 K, to 12.2423(2) Å at 5.5 K, to 12.2414(1) Å at 0.04 K. However, no structural distortion could be detected to within the instrumental resolution.

No magnetic scattering intensity could be resolved on the low-temperature spectra. It is reasonable to expect a magnetic unit cell in the magnetic ordered region (below T_L) of CPS to be of similar structure to the one found in the $Ce_3Pd_{20}Ge_6$ with wave-vector transfer $k=[0,0,1]$.[14]

The vertical bars in Fig. 5(c) indicate the 2*d*-spacing values where magnetic diffraction peaks would be expected for a magnetic propagation vector $k=[0,0,1]$. However, no coherent diffraction intensity could be resolved near these positions. The intensity resolution of the GEM spectrometer puts an upper limit of $\sim 0.2\mu_B$ on the size of an ordered moment in CPS which is similar to the ordered moment found $Ce_3Pd_{20}Ge_6$ in by Dönni *et al.*[14]

III. RESULTS AND DISCUSSION: POLARIZED NEUTRON SCATTERING

The temperature and magnetic field dependence of the magnetic and nuclear Bragg scattering of the ground state of CPS has been probed using uniaxial neutron polarization analysis on the diffuse neutron spectrometer D7, in diffraction mode, at the Institut-Laue-Langevin in Grenoble.[30] An incident wavelength of 3.1 Å was chosen with a pyrolytic graphite monochromator. The incident energy was set to E_I=8.5 meV ensuring complete integration over all CEF transitions. The measurement was performed on a polycrystalline sample, 33.73 g, in applied magnetic fields, perpendicular to the scattering vector, up to 1.5 T over a range of temperatures $0.1<T<10$ K. Additional measurements were performed using a Vanadium standard to calibrate the detector efficiency and a quartz standard to correct the analyzer efficiencies. The Vanadium standard also served as an absolute measure of scattering intensity. A quartz calibration was performed for 0.07, 0.7, 1.1, and 1.5 T. The quartz calibration for other fields was obtained via interpolation.

Uniaxial polarization analysis on D7 measures two scattering cross-sections commonly referred to as nonspin flip (NSF) and spin flip (SF) cross-sections representing an incident neutron polarized along the magnetic field direction with an eigenstate $|+\rangle$ and detected with the same eigenstate (NSF) or with an incident eigenstate $|-\rangle$ detected with a $|+\rangle$ eigenstate (SF). The spin-dependent energy integrated scattering cross-section is given by

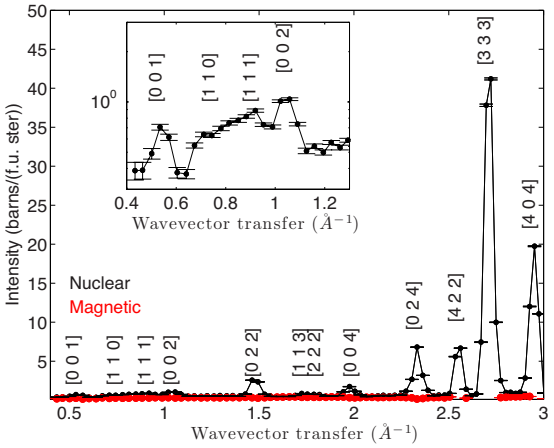

FIG. 6. (Color online) Separation of nuclear and magnetic scattering at 60 mK and 0.07 T measured on D7 with incident wavelength 3.1 Å. The inset shows the nuclear scattering at low wavevector transfer.

$$\frac{d\sigma}{d\Omega}^{z}_{(\mathrm{NSF})} = \frac{d\sigma}{d\Omega}^{\mathrm{nuc}} + \frac{1}{2}\frac{d\sigma}{d\Omega}^{\mathrm{mag}} + \frac{1}{3}\frac{d\sigma}{d\Omega}^{\mathrm{SI}}, \tag{5}$$

$$\frac{d\sigma}{d\Omega}^{z}_{(\mathrm{SF})} = \frac{1}{2}\frac{d\sigma}{d\Omega}^{\mathrm{mag}} + \frac{2}{3}\frac{d\sigma}{d\Omega}^{\mathrm{SI}}. \tag{6}$$

Manipulation of Eqs. (5) and (6) lead to the separation of magnetic (MAG) and nuclear (NUC) scattering cross-sections

$$\frac{d\sigma}{d\Omega}^{\mathrm{NUC}} = \frac{d\sigma}{d\Omega}^{\mathrm{nuc}} - \frac{1}{3}\frac{d\sigma}{d\Omega}^{\mathrm{SI}}, \tag{7}$$

$$\frac{d\sigma}{d\Omega}^{\mathrm{MAG}} = \frac{d\sigma}{d\Omega}^{\mathrm{mag}} + \frac{4}{3}\frac{d\sigma}{d\Omega}^{\mathrm{SI}} \tag{8}$$

from which the nuclear spin incoherent (SI) scattering cannot be separated when performing a uniaxial measurement. In CPS this is a small contribution which, indeed, turned out to be comparably insignificant since the spin incoherent contributions are 0.00(10), 0.093(9), and 0.004(8) barns for Ce, Pd, and Si, respectively. The scattering discussed henceforth will be the MAG and NUC scattering cross-sections from Eqs. (7) and (8) indicating magnetic or nuclear scattering including the minimal SI contribution. The data obtained on D7 provided a temperature dependence at 0.07 T for $0.1<T<800$ mK and a magnetic field dependence at 0.1 K for $0.07<H<1.5$ T. The nuclear scattering is shown in Fig. 6. We have applied the correct atomic sites according to the symmetry operation explained in Sec. II, by which full indexing of the coherent diffraction peaks in the spectrum is achieved.

The temperature dependence of the magnetic scattering at 0.07 T did not reveal any long-range magnetic order down to 0.1 K. At first glance this is surprising due to magnetic neutron evidence of the ordering found in the isostructural $Ce_3Pd_{20}Ge_6$.[14] However the lack of detectable neutron evidence of magnetic order in CPS becomes understandable when the paramagnetic state is analyzed. Single-ion behavior

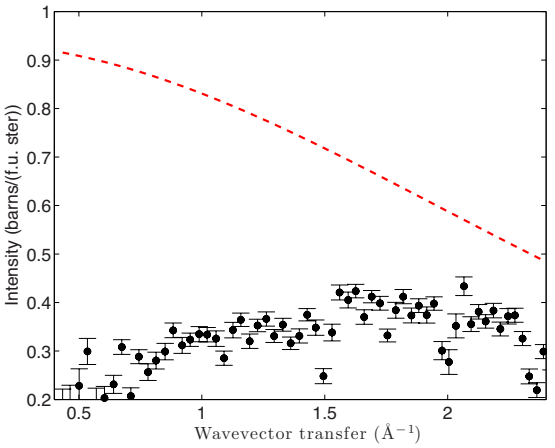

FIG. 7. (Color online) Paramagnetic scattering at 20 K and 0.07 T. The dashed red line is the paramagnetic scattering expected for Ce^{3+}, $J=5/2$, single-ion behavior and the black dots represent scattering observed in $\frac{d\sigma}{d\Omega}$MAG.

in the paramagnetic state gives rise to magnetic neutron scattering of the form

$$\frac{d\sigma}{d\Omega}^{Para} = \sum_{Q} \frac{2}{3} NS(S+1)(r_0\gamma)^2 f^2(Q), \tag{9}$$

where $\frac{2}{3}$ results from the powder average, N is the number of spins, $S=5/2$, for the magnetic ion Ce^{3+} per formula unit, $r_0\gamma=-0.54\times10^{12}$ cm and $f(Q)$ is the magnetic form factor of Ce^{3+}.[22] The paramagnetic state was probed at 20 K and 0.07 T, Fig. 7 with the black dots representing the magnetic scattering observed while the red dashed line is the paramagnetic scattering expected for the full Ce^{3+} single-ion moment. It is clear that the magnetic scattering observed is not consistent with the expected paramagnetic scattering and furthermore the intensity observed can be accounted for by spin incoherent scattering, thus no magnetic scattering is observed. On D7 the energy window probed by the neutrons is limited by the incoming energy of the neutrons, $E_i=8.5$ meV in this case. The diffraction data is composed of the integrated intensity over that energy window. If the magnetic scattering is more dynamic than this energy window this magnetic scattering cannot be probed and will be observed as missing intensity. It can thus only be assumed that the missing scattering lies outside the window of energy probed by D7.

In contrast, unusual magnetic field induced short-range magnetic scattering appears at low temperatures, $T=60$ mK, around the reciprocal space position $Q=0.82(5)$ Å^{-1}, Fig. 8(a). There are a number of interesting features that can be observed. First, the maximum intensity of the scattering increases up to about 1.2 T which is close to the field which drives CPS to a QCP.[17] However, the correlation length decreases as a function of field with a correlation length $D=2\pi/\Delta Q=213(14)$ Å at 1.1 T which diminishes by an order of magnitude at 1.5 T.

At present it is not possible, due to experimental limits, to ascertain whether the diffuse magnetic scattering is due to magnetic quantum-critical fluctuations and is thus of an in-

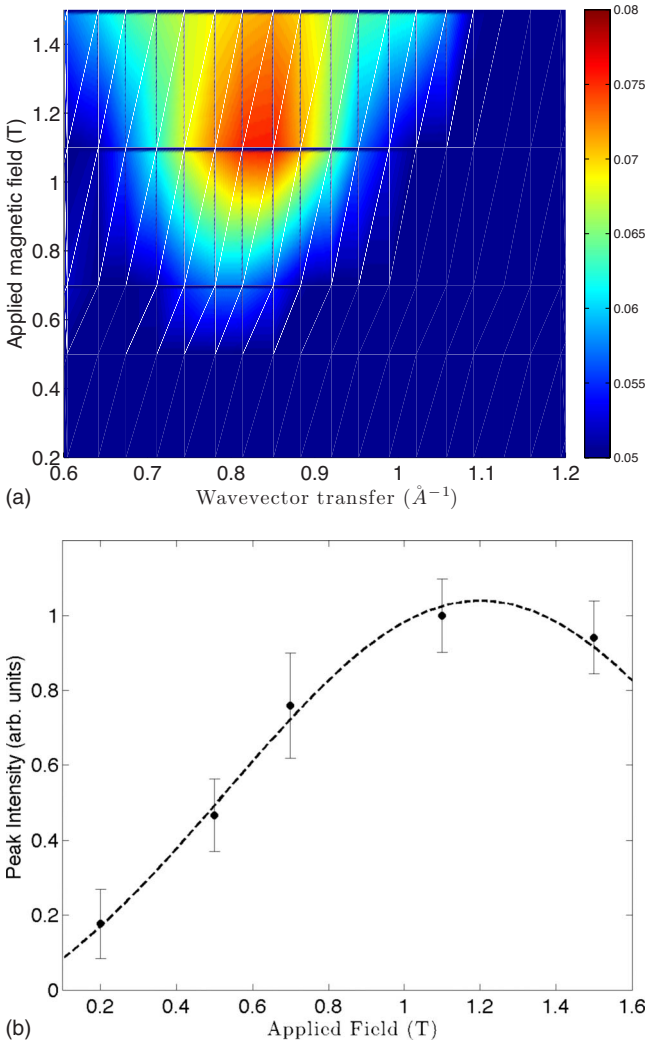

FIG. 8. (Color online) (a) Contour plot of the broad diffuse magnetic scattering around the reciprocal space position of $Q=0.82(3)$ Å^{-1}. (b) The maximum intensity as a function of applied magnetic field showing the most intense scattering close to the critical field of approximately 1.1 T.

elastic nature or whether it is due to static magnetic short-range order. Short-range magnetic correlations in a powder sample scatter according to the expression

$$\frac{d\sigma}{d\Omega}^{\text{mag}} \sim \sum_{n} \frac{\langle \mathbf{S_0}\cdot\mathbf{S_n}\rangle}{S(S+1)} N_n \frac{\sin(QR_n)}{QR_n}, \tag{10}$$

where S_0 and S_n are the spin magnitudes of the central atom and the nth shell atom. R_n and N_n are the radii and coordination numbers of the nth nearest-neighbor shell, respectively.[31] Figure 9 shows the calculated magnetic correlations due to Ce1-Ce1($4a$), Ce2-Ce2($8c$), or Ce1-Ce2($4a$-$8c$) nearest-neighbor magnetic correlations only, with a net antiferromagnetic order across the shell. By comparing the calculated magnetic neutron-scattering cross-sections of various origins in Fig. 9 with the observed scattering shown in Fig. 8 we are able to identify Ce1-Ce1 interactions, Fig. 9 blue line, as the least likely contribution to the weighted magnetic scattering. A pure Ce2-Ce2 interaction,

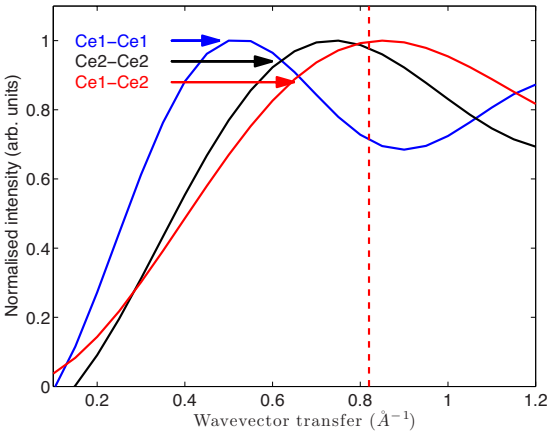

FIG. 9. (Color online) Magnetic scattering cross-sections expected due to nearest-neighbor correlations only between Ce1-Ce1, Ce2-Ce2, and Ce1-Ce2 atoms. Dashed line shows the position of the maximum in magnetic scattering from Fig. 8(a).

Fig. 8 black line, is somewhat more likely, but from our analyses the mixed Ce1-Ce2 interaction between the two different Ce sites, Fig. 8 red line, has to be considered as the most probable magnetic interaction responsible for the neutron-scattering cross-section at $Q \simeq 0.82$ Å^{-1} in CPS at its QCP.

IV. CONCLUSION

This study, as well as former work, on the intermetallic compound CPS has shown it to be an *f*-electron magnetic system that is rich in physics and exceptionally complex in the composure of its ground state. Here we have provided a detailed study of its ground state by elastic, inelastic, and polarized neutron scattering. In contrast to the other rare-earth ternary intermetallic series, $RE\mathrm{Pd}_{20}\mathrm{Ge}_6$, the two inequivalent Ce sites in CPS ($4a$ and $8c$) also possess inequivalent ground states, Γ_7 and Γ_8, respectively. Symmetry indicates that a Γ_7 ground state can only lead to dipolar order while a Γ_8 ground state allows for multipolar order. The transition at T_U of Ce at the $8c$ sites might thus be a quadrupolar transition, while the one of Ce at the $4a$ site at T_L can only be magnetic in origin. Furthermore, the transition at T_U was shown to affect the crystal field around the $4a$ magnetic site indicating a sizable interaction between the Ce atoms at $4a$ and $8c$.

Recent work[32] hypothesized that the ground state of the $4a$ site may fall into a singlet state screened by conduction electrons at low temperatures without long-range magnetic ordering. Our work has also not obtained a direct observation of long-range magnetic order. However, field-induced diffuse magnetic scattering was observed at 60 mK with maximum intensity at approximately 1.2 T, close to the field that induces a QCP, with spatial correlations indicative of Ce1-Ce2 correlations. These observations lead to the conclusion that long-range magnetic order does exist below 0.3 K and at 0 T but have an energy scale greater than the energy measured on D7, 8.5 meV.

Our analyses of diffuse neutron scattering furthermore elucidates aspects of quantum criticality which we believe may be of central importance in understanding the dynamics of the suppression and eventual extinction of magnetic order that leads to quantum criticality. The diffuse magnetic scattering is shown to reach an apex right at the critical field of the quantum critical point. Further studies are highly required to shed light on temperature and field scalings of the diffuse magnetic scattering itself, as these may lead to further significant probes of quantum criticality.

ACKNOWLEDGMENTS

We thank B. Rainford for fruitful discussions. A.M.S. thanks the SA-NRF (Grant No. 2072956) and the University of Johannesburg Research Committee for funding support. S.P. acknowledges the financial support by the ERC Advanced under Grant No. 227378 and the Austrian Science fund (FWF, Grant No. P19458).

[1] H. v. Löhneysen, A. Rosch, M. Vojta, and P. Wölfle, Rev. Mod. Phys. **79**, 1015 (2007).
[2] P. Gegenwart, Q. Si, and F. Steglich, Nat. Phys. **4**, 186 (2008).
[3] N. Takeda, J. Kitagawa, and M. Ishikawa, J. Phys. Soc. Jpn. **64**, 387 (1995).
[4] A. Amato, D. Jaccard, J. Flouquet, F. Lapierre, J. L. Tholence, R. A. Fisher, S. E. Lacey, J. Olsen, and N. Phillips, J. Low Temp. Phys. **68**, 371 (1987).
[5] A. M. Strydom, A. Pikul, F. Steglich, and S. Paschen, J. Phys.: Conf. Ser. **51**, 239 (2006).
[6] S. Paschen, *in Thermoelectrics Handbook*, edited by D. M. Rowe (CRC, Taylor & Francis Group, Boca Raton, 2006), Chap. 15.
[7] A. V. Gribanov, Y. D. Seropegin, and O. I. Bodak, J. Alloys Compd. **204**, L9 (1994).
[8] J. Kitagawa, N. Takeda, and M. Ishikawa, J. Alloys Compd. **256**, 48 (1997).
[9] A. Dönni, L. Keller, P. Fischer, Y. Aoki, H. Sato, F. Fauth, M. Zolliker, T. Komatsubara, and Y. Endoh, J. Phys.: Condens. Matter **10**, 7219 (1998).
[10] N. Kimura, N. Tateiwa, M. Nakayama, H. Aoki, T. Komatsubara, T. Sakon, M. Motokawa, Y. Koike, and N. Metoki, Physica B **259-261**, 338 (1999).
[11] T. Hermannsdörfer, A. Dönni, P. Fischer, L. Keller, G. B. Böttger, M. Gutmann, H. Kitazawa, and J. Tang, J. Phys.: Condens. Matter **11**, 2929 (1999).
[12] T. Hermannsdörfer, A. Dönni, P. Fischer, L. Keller, E. Clementyev, A. Furrer, S. Mango, B. van den Brandt, and H. Kitazawa, J. Alloys Compd. **323-324**, 509 (2001).
[13] J. Kitagawa, N. Takeda, and M. Ishikawa, Phys. Rev. B **53**, 5101 (1996).
[14] A. Dönni, T. Herrmannsdorfer, P. Fischer, L. Keller, F. Fauth, K. McEwen, T. Goto, and T. Komatsubara, J. Phys.: Condens. Matter **12**, 9441 (2000).

[15] T. Goto, T. Horino, Y. Nemoto, T. Yamaguchi, A. Dönni, O. Suzuki, and T. Komatsubara, Physica B **312-313**, 492 (2002).
[16] V. N. Duginov, K. I. Gritsaj, A. Amato, C. Baines, D. Herlach, V. Y. Pomjakushin, U. Zimmermann, A. N. Ponomarev, I. A. Krivosheev, A. A. Nezhivoy, A. V. Gribanovd, V. N. Nikiforovd, and Yu. D. Seropegin, Physica B **289-290**, 43 (2000).
[17] S. Paschen, M. Müller, J. Custers, M. Kriegisch, A. Prokofiev, G. Hilscher, W. Steiner, A. Pikul, F. Steglich, and A. Strydom, J. Magn. Magn. Mater. **316**, 90 (2007).
[18] K. W. H. Stevens, Proc. Phys. Soc., London, Sect. A **65**, 209 (1952).
[19] K. R. Lea, M. J. M. Leask, and W. P. Wolf, J. Phys. Chem. Solids **23**, 1381 (1962).
[20] M. T. Hutchings, Solid State Phys. **16**, 227 (1964).
[21] G. L. Squires, *Introduction to the Theory of Thermal Neutron Scattering* (Dover, New York, 1978).
[22] P. J. Brown, in *International Tables for Crystallography*, Vol. C (Kluwer Academic, Dordrecht, The Netherlands, 2006).
[23] S. Paschen, S. Laumann, A. Prokofiev, A. M. Strydom, P. P. Deen, J. R. Stewart, K. Neumaier, A. Goukassov, and J.-M. Mignot, Physica B **403**, 1306 (2008).
[24] N. E. Bickers, D. L. Cox, and J. W. Wilkins, Phys. Rev. Lett. **54**, 230 (1985).
[25] E. A. Goremychkin and R. Osborn, Phys. Rev. B **47**, 14280 (1993).
[26] A. P. Murani, *Theoretical and Experimental Aspects of Valence Fluctuations and Heavy Fermions*, edited by L. C. Gupta and S. K. Malik (Plenum, New York, 1987), p. 287.
[27] E. A. Goremychkin and R. Osborn, Phys. Rev. B **47**, 14580 (1993).
[28] L. Keller, A. Dönni, M. Zolliker, and T. Komatsubara, Physica B **259-261**, 336 (1999).
[29] Th. Hahn in *International Tables for Crystallography*, Vol. A (Kluwer Academic, Dordrecht, The Netherlands, 2006).
[30] J. R. Stewart, P. P. Deen, K. H. Andersen, H. Schober, J.-F. Barthélémy, J. M. Hillier, A. P. Murani, T. Hayes, and B. Lindenau, J. Appl. Crystallogr. **42**, 69 (2009).
[31] B. D. Rainford, J. Phys. (France) **43**, C7 (1982).
[32] T. Goto, T. Watanabe, O. Suzuki, H. Kobayashi, Y. Nemoto, N. Takeda, A. Donni, and H. Kitazawa, J. Phys. Soc. Jpn. **78**, 024716 (2009).